Supplementary Materials: Targeted Metabolomics Identifies Plasma Biomarkers in Mice with Metabolically Heterogeneous Melanoma Xenografts

Daniela D Weber, Maheshwor Thapa, Sepideh Aminzadeh-Gohari, Anna-Sophia Redtenbacher, Luca Catalano, René G Feichtinger, Peter Koelblinger, Guido Dallmann, Michael Emberger, Barbara Kofler and Roland Lang

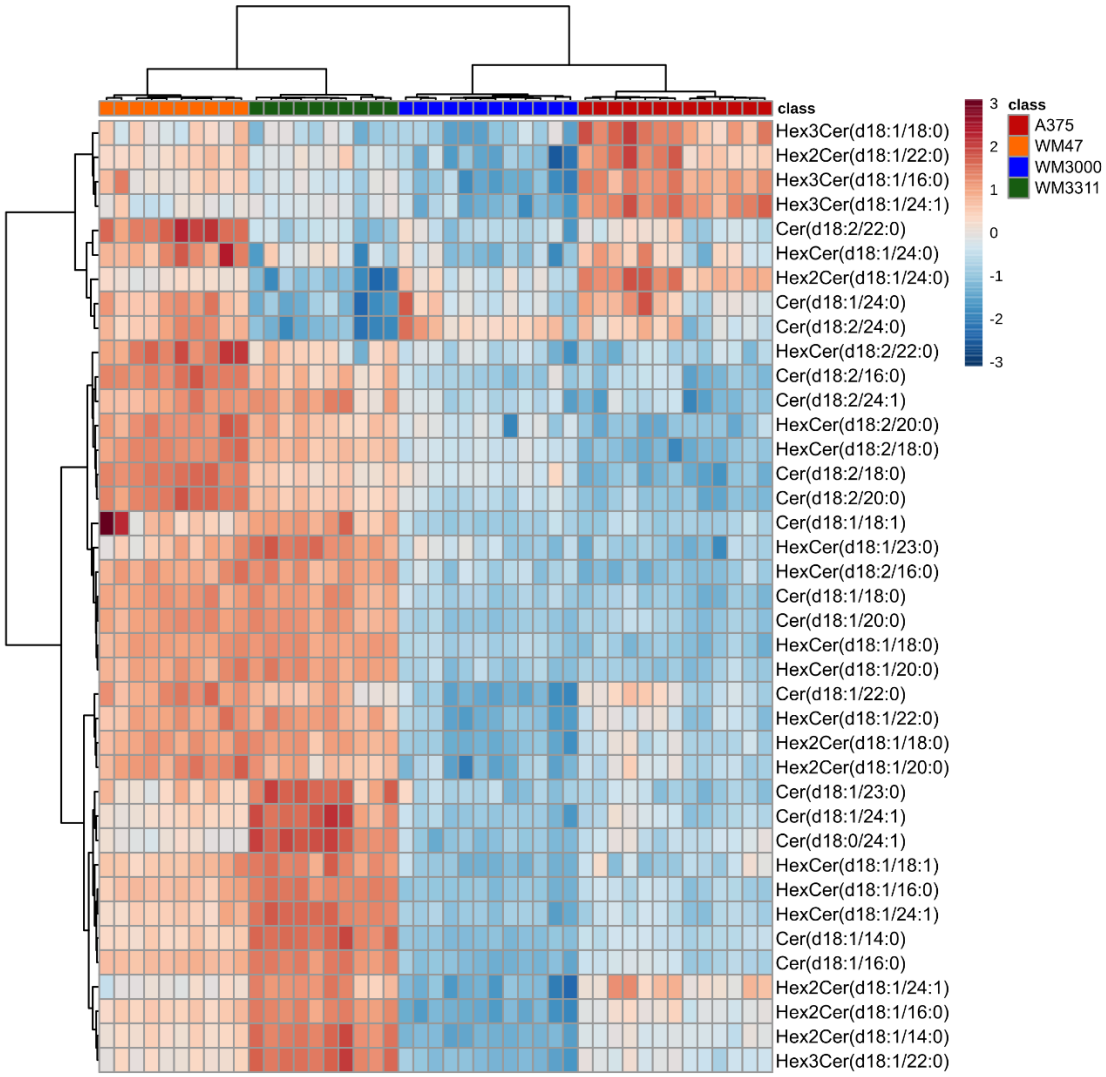

Figure S1. Hierarchical clustering of ceramides, dihydroceramides, hexosylceramides, di- and trihexosylceramides quantified in A375-, WM47-, WM3000-, and WM3311-melanoma xenografts. *n* = 10–13; Cx:y: x = number of carbons in the fatty acid side chain and y = number of double bonds in the fatty acid side chain, Cer: ceramide, HexCer: hexosylceramide, Hex2Cer: dihexosylceramide, Hex3Cer: trihexosylceramide.

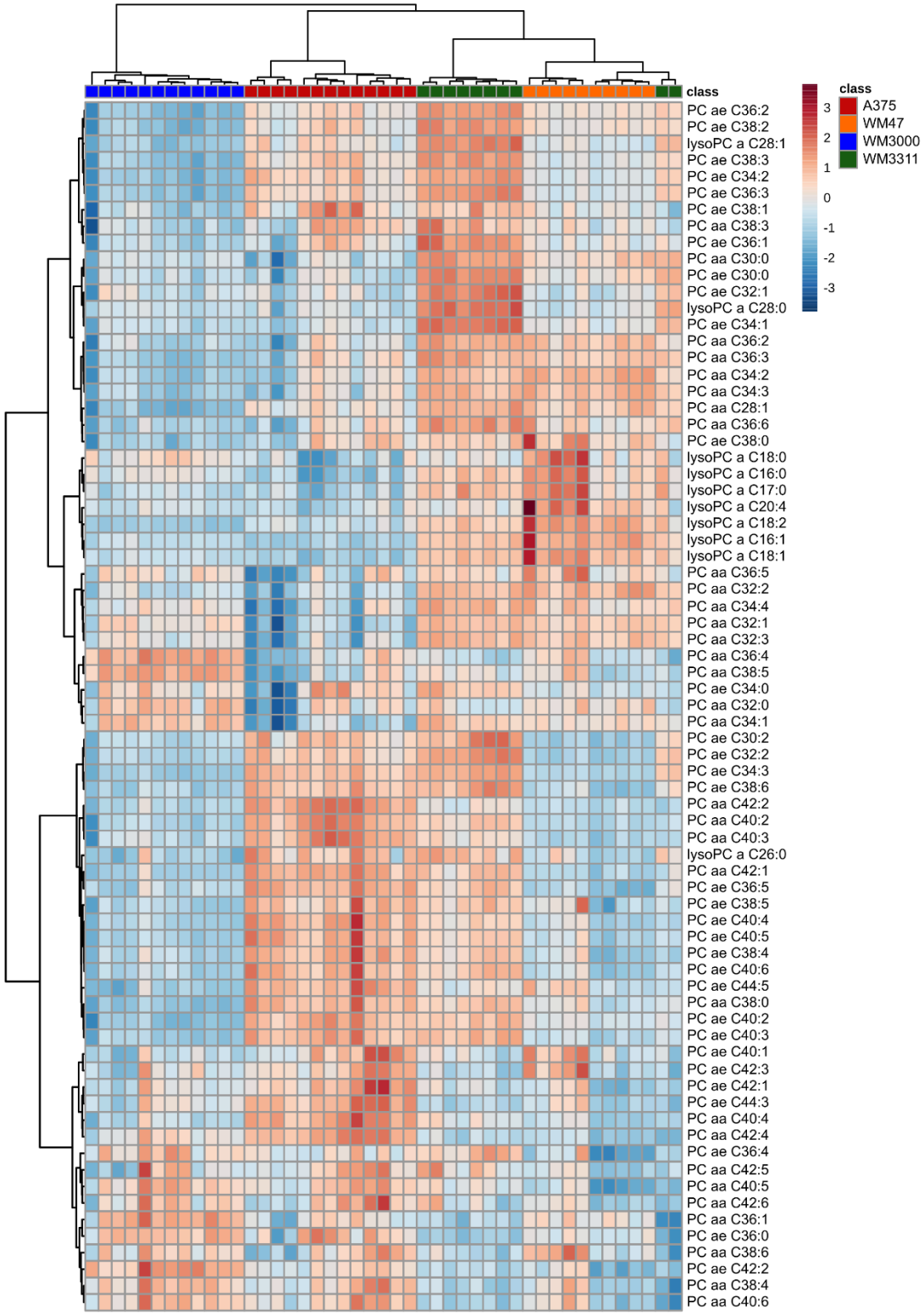

Figure S2. Hierarchical clustering of phosphatidylcholines and lyso-phosphatidylcholines quantified in A375-, WM47-, WM3000-, and WM3311-melanoma xenografts. *n* = 10–13; aa: acyl-acyl, ae: acyl-alkyl, Cx:y: x = number of carbons in the fatty acid side chain and y = number of double bonds in the fatty acid side chain, lysoPC: lyso-phosphatidylcholine, PC: phosphatidylcholine.

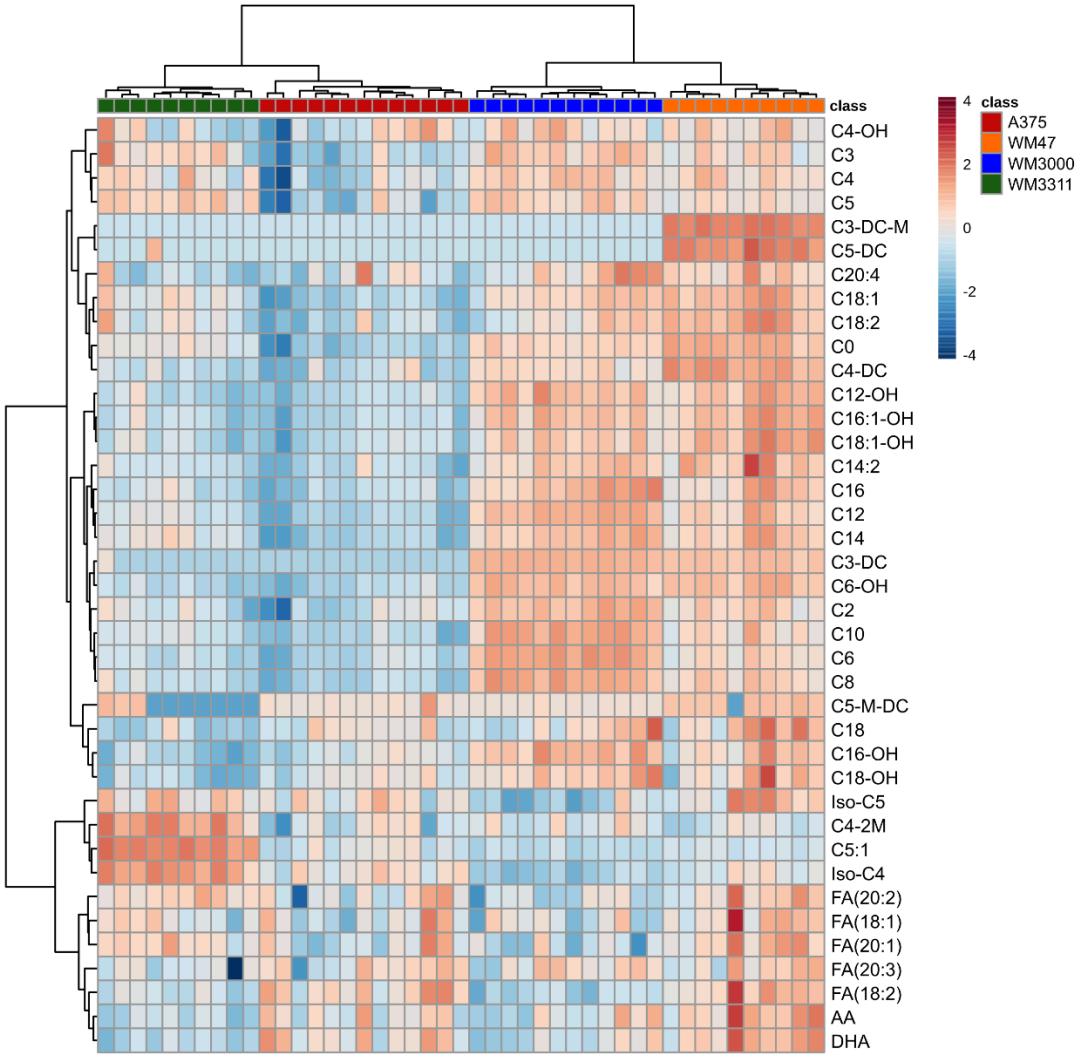

Figure S3. Hierarchical clustering of fatty acids and acylcarnitines quantified in A375-, WM47-, WM3000-, and WM3311-melanoma xenografts. *n* = 10–13; Cx:y: x = number of carbons in the fatty acid side chain and y = number of double bonds in the fatty acid side chain, AA: arachidonic acid, C0: carnitine, C2: acetylcarnitine, C3: propionylcarnitine, C3-DC: malonylcarnitine, C3-DC-M: methylmalonylcarnitine, C4: butyrylcarnitine, C4-2M: 2-methylbutyrylcarnitine, C4-DC: succinylcarnitine, C4-OH: hydroxybutyrylcarnitine, C5: valerylcarnitine, C5-DC: glutarylcarnitine, C5-M-DC: methylglutarylcarnitine, C5:1: tiglylcarnitine, C6: hexanoylcarnitine, C6-OH: hydroxyhexanoyl-carnitine, C8: octanoylcarnitine, C10: decanoylcarnitine, C12: dodecanoylcarnitine, C12-OH: hydroxydodecanoylcarnitine, C14: tetradecanoylcarnitine, C14:2: tetradecadienoylcarnitine, C16: hexadecanoylcarnitine, C16-OH: hydroxyhexadecanoylcarnitine, C16:1-OH: hydroxyhexadecenoyl-carnitine, C18: octadecanoylcarnitine, C18-OH: hydroxyoctadecanoylcarnitine, C18:1: octadecenoyl-carnitine, C18:1-OH: hydroxyoctadecenoylcarnitine, C18:2: octadecadienylcarnitine, C20:4: arachidonyl-carnitine, DHA: docosahexaenoic acid, FA(18:1): octadecenoic acid, FA(18:2): octadecadienoic acid, FA(20:1): eicosenoic acid, FA(20:2): eicosadienoic acid, FA(20:3): eicosatrienoic acid, Iso-C4: iso-butyrylcarnitine, Iso-C5: iso-valerylcarnitine.

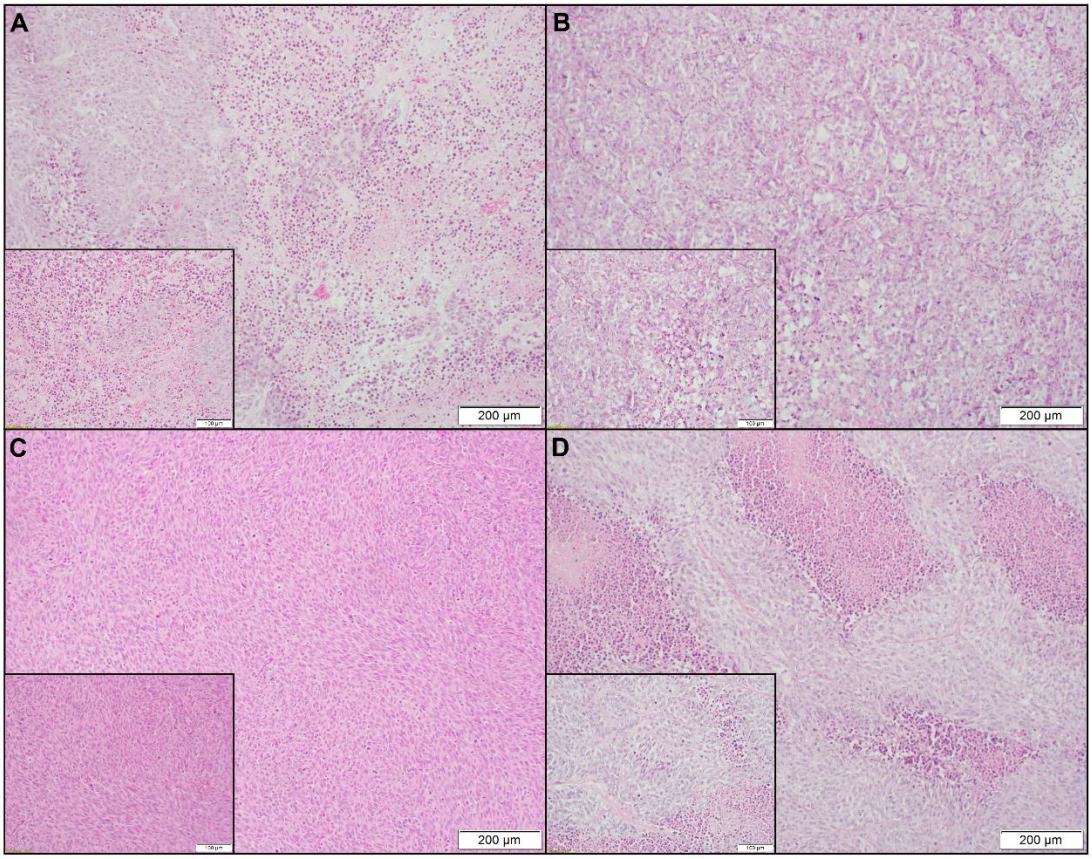

Figure S4. Histological analysis of melanoma xenograft tissues. Hematoxylin and eosin (HE) staining of (**A**) A375-, (**B**) WM47-, (**C**) WM3000-, and (**D**) WM3311-melanoma xenograft tissues; the large and the small images show 10× and 20× magnification, respectively. A375- and WM47-xenografts carry the same BRAF mutation and were cytologically similar but different in terms of the size of epithelioid cells, the extent of eosinophilic cytoplasm and amount of necrosis. NRAS mutant WM3000-xenografts were characterized by a sarcoma-like pattern, which clearly distinguishes this tumor from the other three. Distinctive features of the triple-wild-type WM3311-xenografts were the pleomorphic cytology and the clear separation of vital and necrotic tumor areas within the tumor.

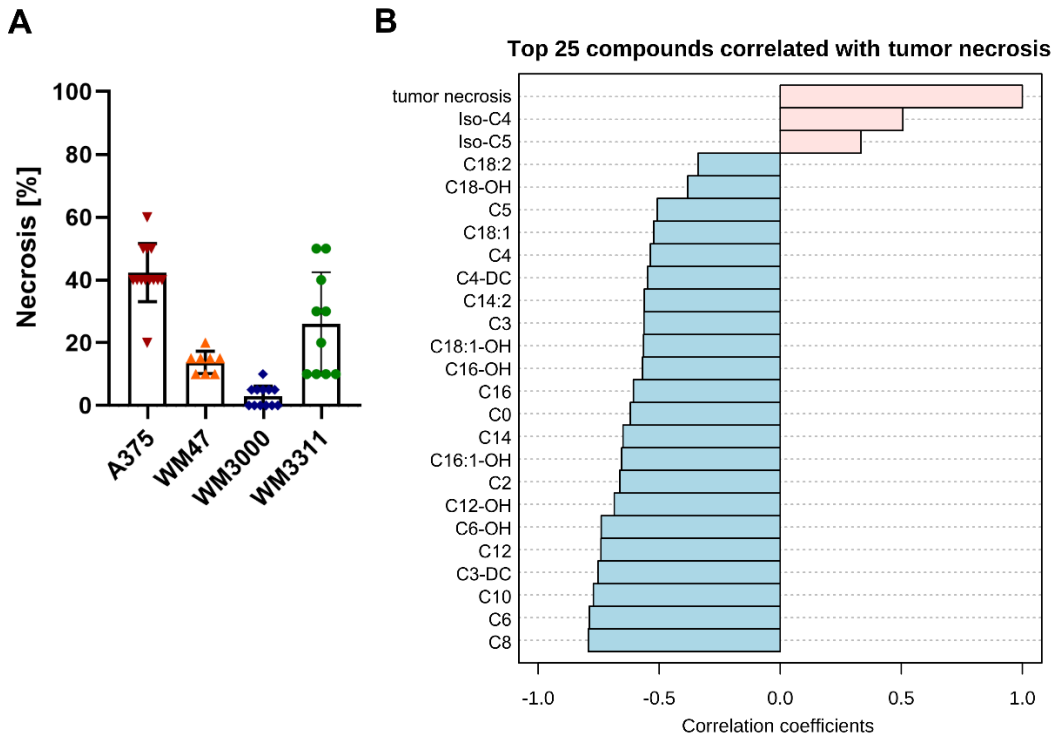

Figure S5. Negative correlations between tumor necrosis and acylcarnitines in melanoma xenografts. (**A**) Percentage of necrosis in melanoma xenografts, $n = 8–13$. (**B**) Top 25 acylcarnitines correlated with tumor necrosis; Pearson correlation coefficient $r > 0$ indicates a positive correlation, whereas $r < 0$ indicates a negative correlation.

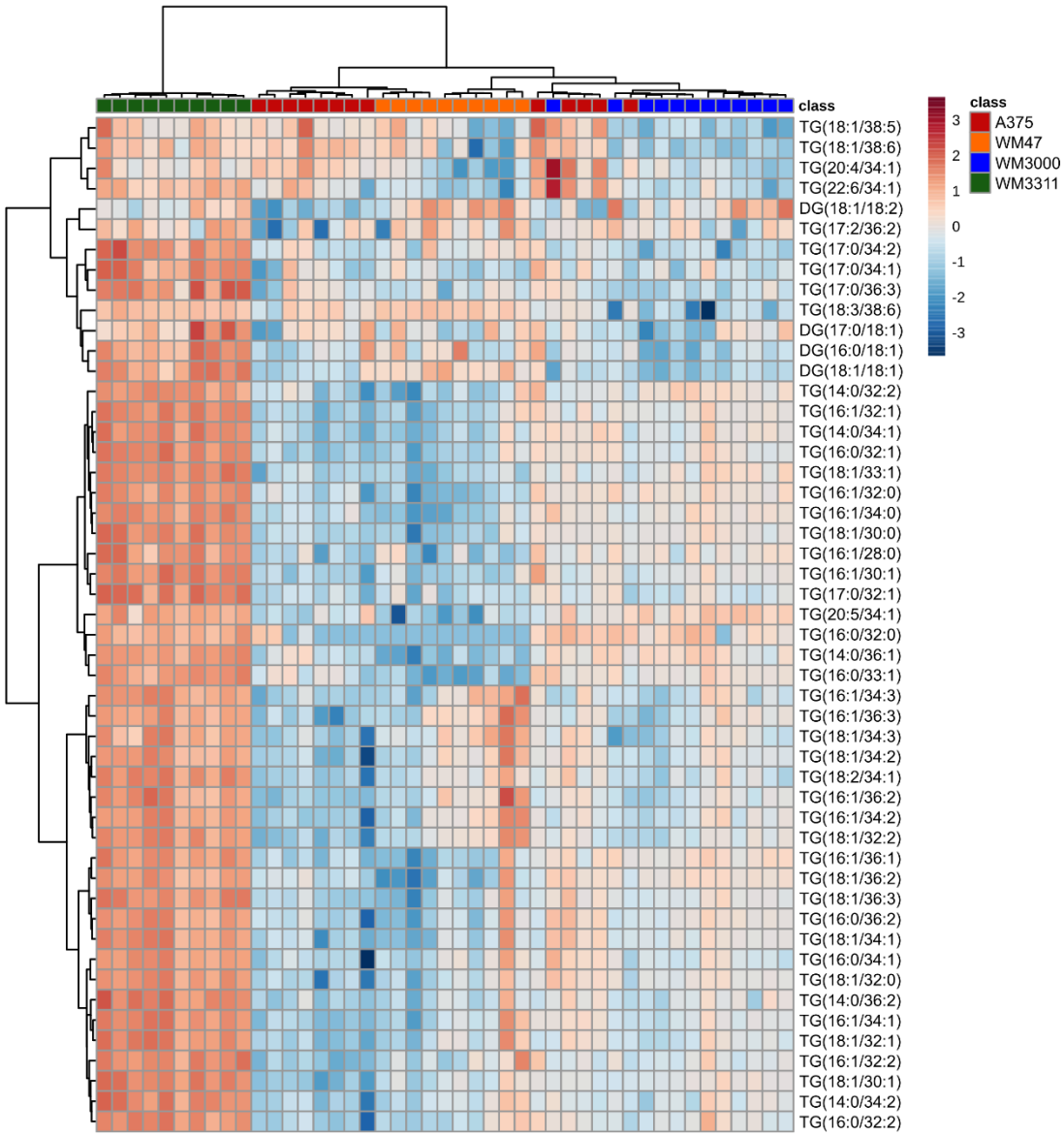

Figure S6. Hierarchical clustering of di- and triglycerides quantified in A375-, WM47-, WM3000-, and WM3311-melanoma xenografts. *n* = 10–13; aa: Cx:y: x = number of carbons in the fatty acid side chain and y = number of double bonds in the fatty acid side chain, DG: diglyceride, TG: triglyceride.

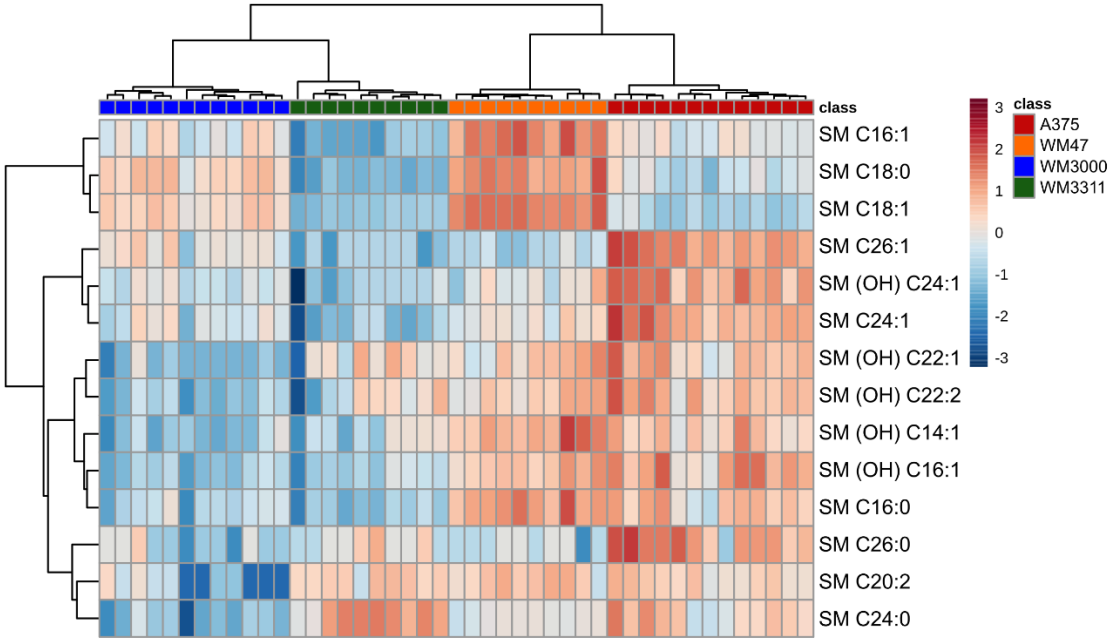

Figure S7. Hierarchical clustering of sphingomyelins quantified in A375-, WM47-, WM3000-, and WM3311-melanoma xenografts. *n* = 10–13; aa: Cx:y: x = number of carbons in the fatty acid side chain and y = number of double bonds in the fatty acid side chain, SM: sphingomyelin.

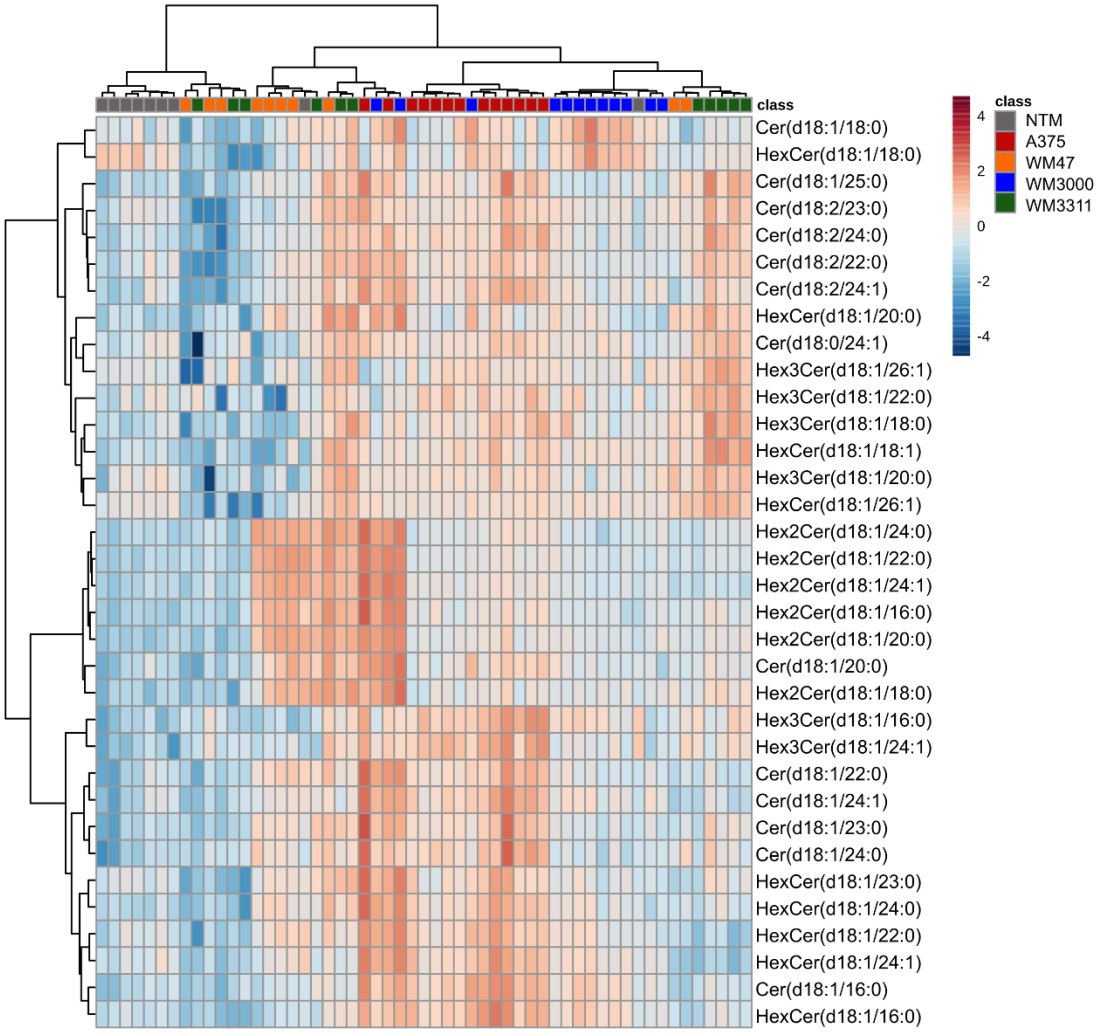

Figure S8. Hierarchical clustering of ceramides, dihydroceramides, hexosylceramides, di- and trihexosylceramides quantified in plasma from A375-, WM47-, WM3000-, or WM3311-melanoma-bearing mice and non-tumor mice (NTM). *n* = 9–13; Cx:y: x = number of carbons in the fatty acid side chain and y = number of double bonds in the fatty acid side chain, Cer: ceramide, HexCer: hexosylceramide, Hex2Cer: dihexosylceramide, Hex3Cer: trihexosylceramide.

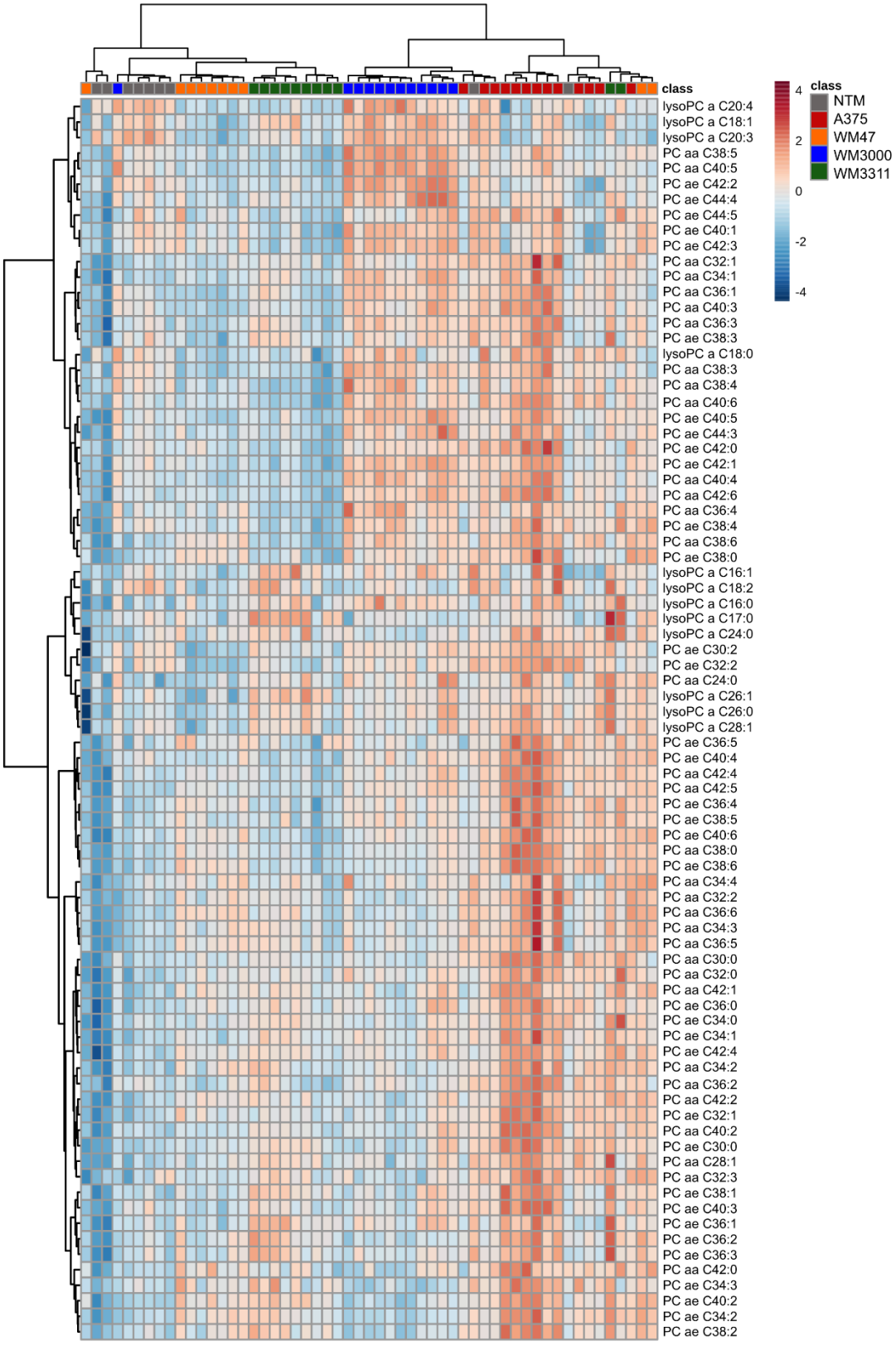

Figure S9. Hierarchical clustering of phosphatidylcholines and lyso-phosphatidylcholines quantified in plasma from A375-, WM47-, WM3000-, or WM3311-melanoma-bearing mice and non-tumor mice (NTM). *n* = 9–13; aa: acyl-acyl, ae: acyl-alkyl, Cx:y: x = number of carbons in the fatty acid side chain and y = number of double bonds in the fatty acid side chain, lysoPC: lyso-phosphatidylcholine, PC: phosphatidylcholine.

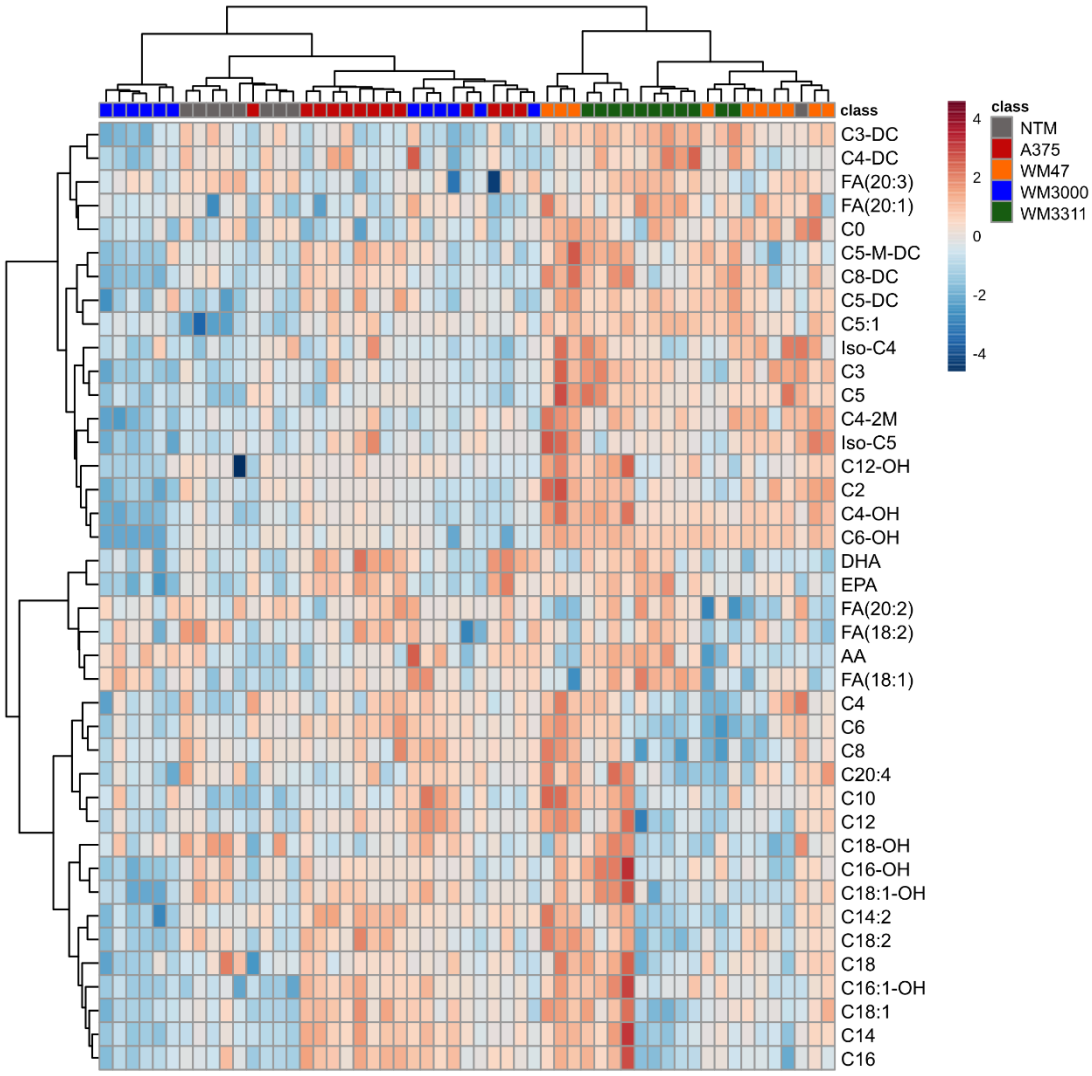

Figure S10. Hierarchical clustering of fatty acids and acylcarnitines quantified in plasma from A375-, WM47-, WM3000-, or WM3311-melanoma-bearing mice and non-tumor mice (NTM). *n* = 9–13; Cx:y: x = number of carbons in the fatty acid side chain and y = number of double bonds in the fatty acid side chain, C0: carnitine, C2: acetylcarnitine, C3: propionylcarnitine, C3-DC: malonylcarnitine, C4: butyrylcarnitine, C4-2M: 2-methylbutyrylcarnitine, C4-DC: succinylcarnitine, C4-OH: hydroxybutyrylcarnitine, C5: valerylcarnitine, C5-DC: glutarylcarnitine, C5-M-DC: methylglutaryl-carnitine, C5:1: tiglylcarnitine, C6: hexanoylcarnitine, C6-OH: hydroxyhexanoylcarnitine, C8: octanoylcarnitine, C8-DC: suberyl-carnitine, C10: decanoylcarnitine, C12: dodecanoylcarnitine, C12-OH: hydroxydodecanoylcarnitine, C14: tetradeca-noylcarnitine, C14:2: tetradecadienoylcarnitine, C16: hexadecanoylcarnitine, C16-OH: hydroxyhexadecanoylcarnitine, C16:1-OH: hydroxyhexadecenoyl-carnitine, C18: octadecanoylcarnitine, C18-OH: hydroxyoctadecanoylcarnitine, C18:1: octadecenoyl-carnitine, C18:1-OH: hydroxyoctadecenoylcarnitine, C18:2: octadecadienylcarnitine, C20:4: arachidonyl-carnitine, DHA: docosahexaenoic acid, EPA: eicosapentaenoic acid, FA(18:1): octadecenoic acid, FA(18:2): octadecadienoic acid, FA(20:1): eicosenoic acid, FA(20:2): eicosadienoic acid, FA(20:3): eicosatrienoic acid, Iso-C4: iso-butyrylcarnitine, Iso-C5: iso-valerylcarnitine.

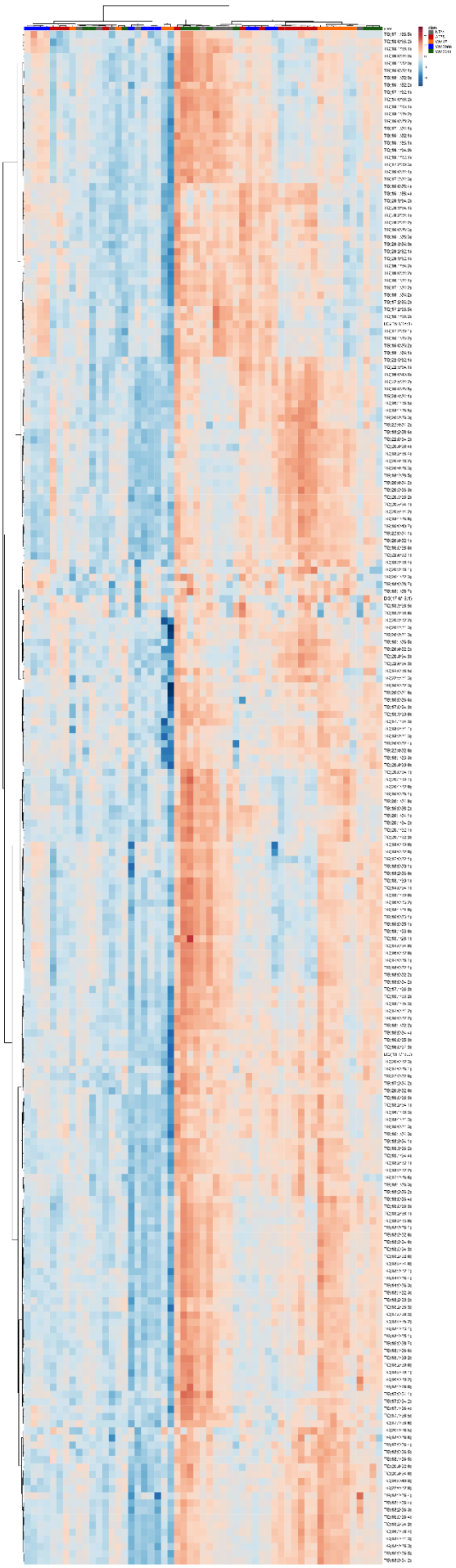

Figure S11. Hierarchical clustering of di- and triglycerides quantified in plasma from A375-, WM47-, WM3000-, or WM3311-melanoma-bearing mice and non-tumor mice (NTM). *n* = 9–13; Cx:y: x = number of carbons in the fatty acid side chain and y = number of double bonds in the fatty acid side chain, DG: diglyceride, TG: triglyceride.

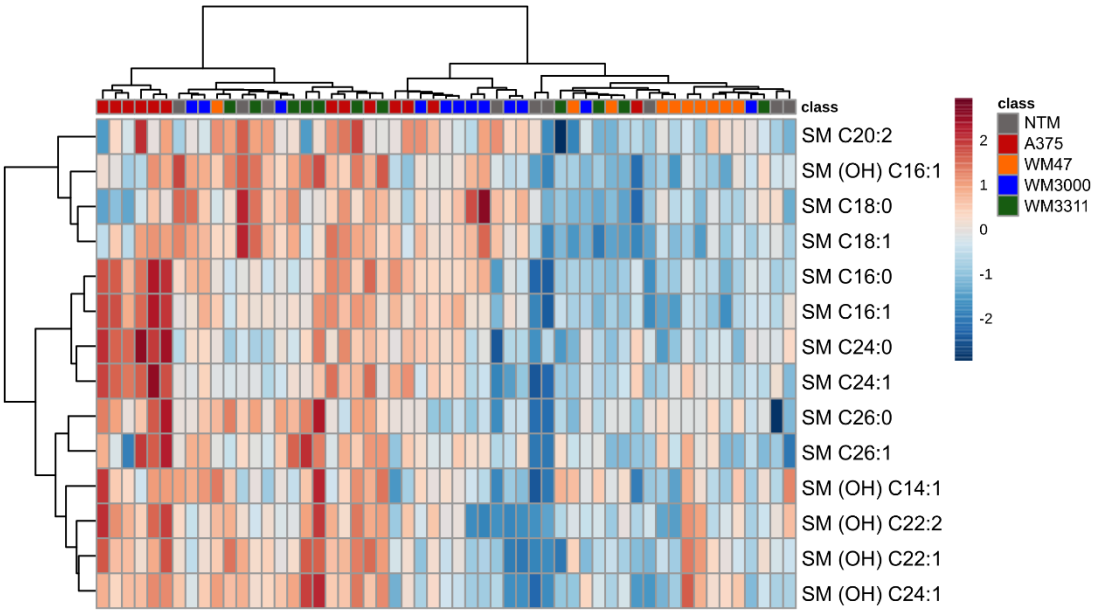

Figure S12. Hierarchical clustering of sphingomyelins quantified in plasma from A375-, WM47-, WM3000-, or WM3311-melanoma-bearing mice and non-tumor mice (NTM). *n* = 9–13; Cx:y: x = number of carbons in the fatty acid side chain and y = number of double bonds in the fatty acid side chain, SM: sphingomyelin.

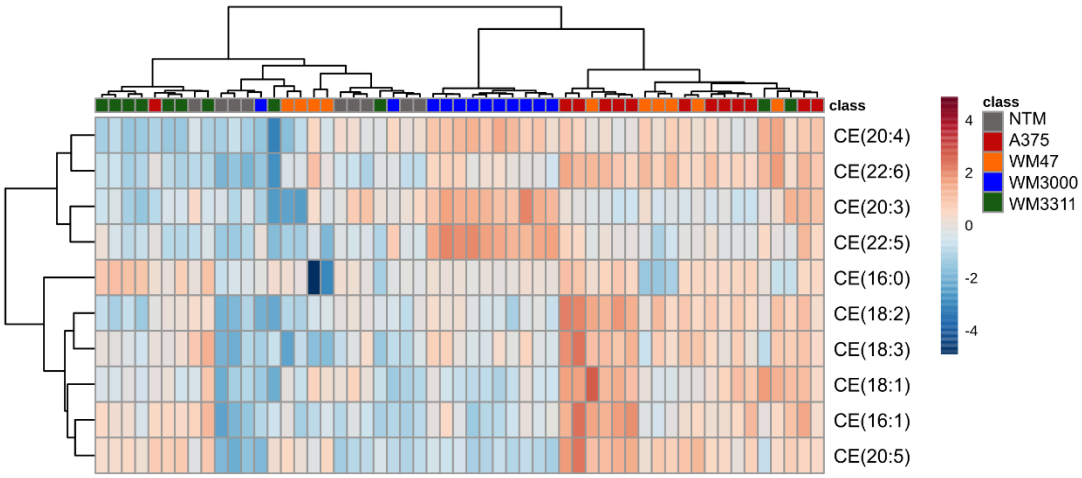

Figure S13. Hierarchical clustering of cholesteryl esters quantified in plasma from A375-, WM47-, WM3000-, or WM3311-melanoma-bearing mice and non-tumor mice (NTM). *n* = 9–13; Cx:y: x = number of carbons in the fatty acid side chain and y = number of double bonds in the fatty acid side chain, CE: cholesteryl ester.

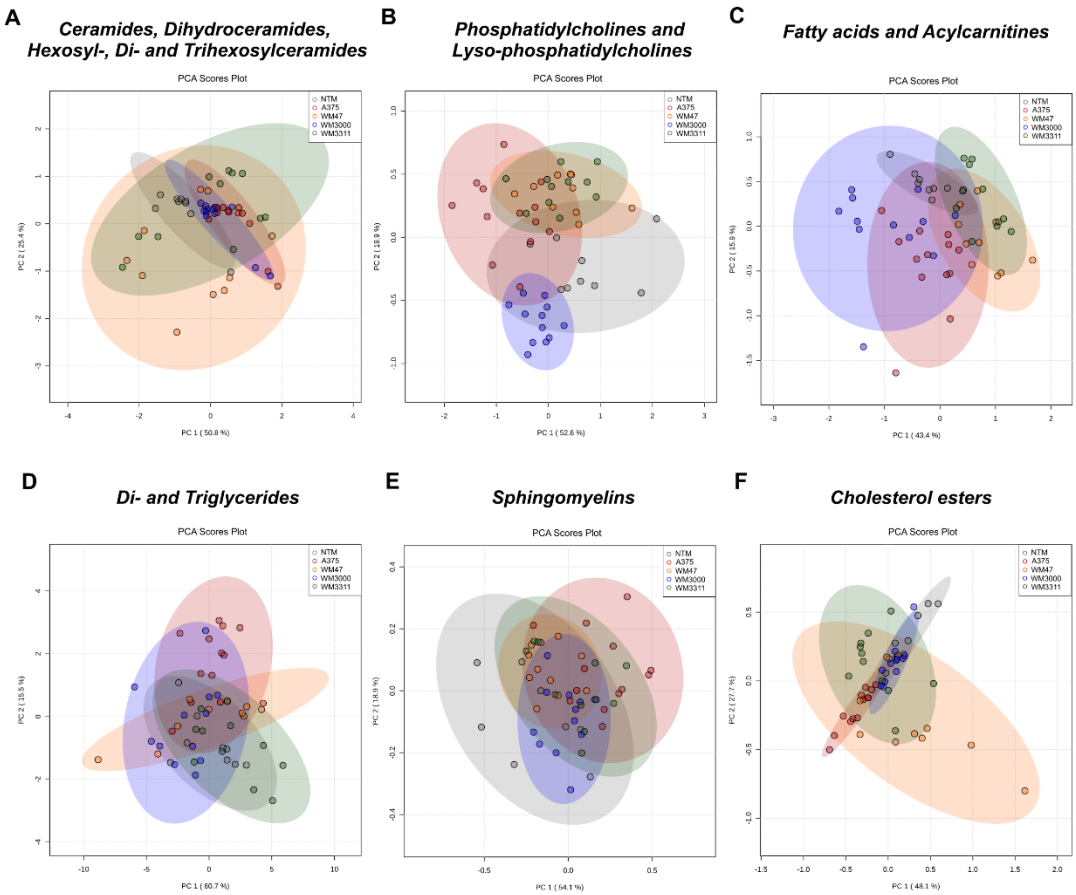

Figure S14. Metabolic analysis of lipid-subclasses in plasma. PCA scores derived from lipid and lipid-like metabolite profiling data of plasma samples from mice bearing A375-, WM47-, WM3000-, and WM3311-melanoma xenografts and non-tumor mice (NTM) divided in lipid-subclasses: (**A**) ceramides, dihydroceramides, hexosylceramides, di- and trihexosylceramides, (**B**) phosphatidylcholines and lyso-phosphatidylcholines, (**C**) fatty acids and acylcarnitines, (**D**) di- and triglycerides, (**E**) sphingomyelins, and (**F**) cholesteryl esters; n = 9–13.

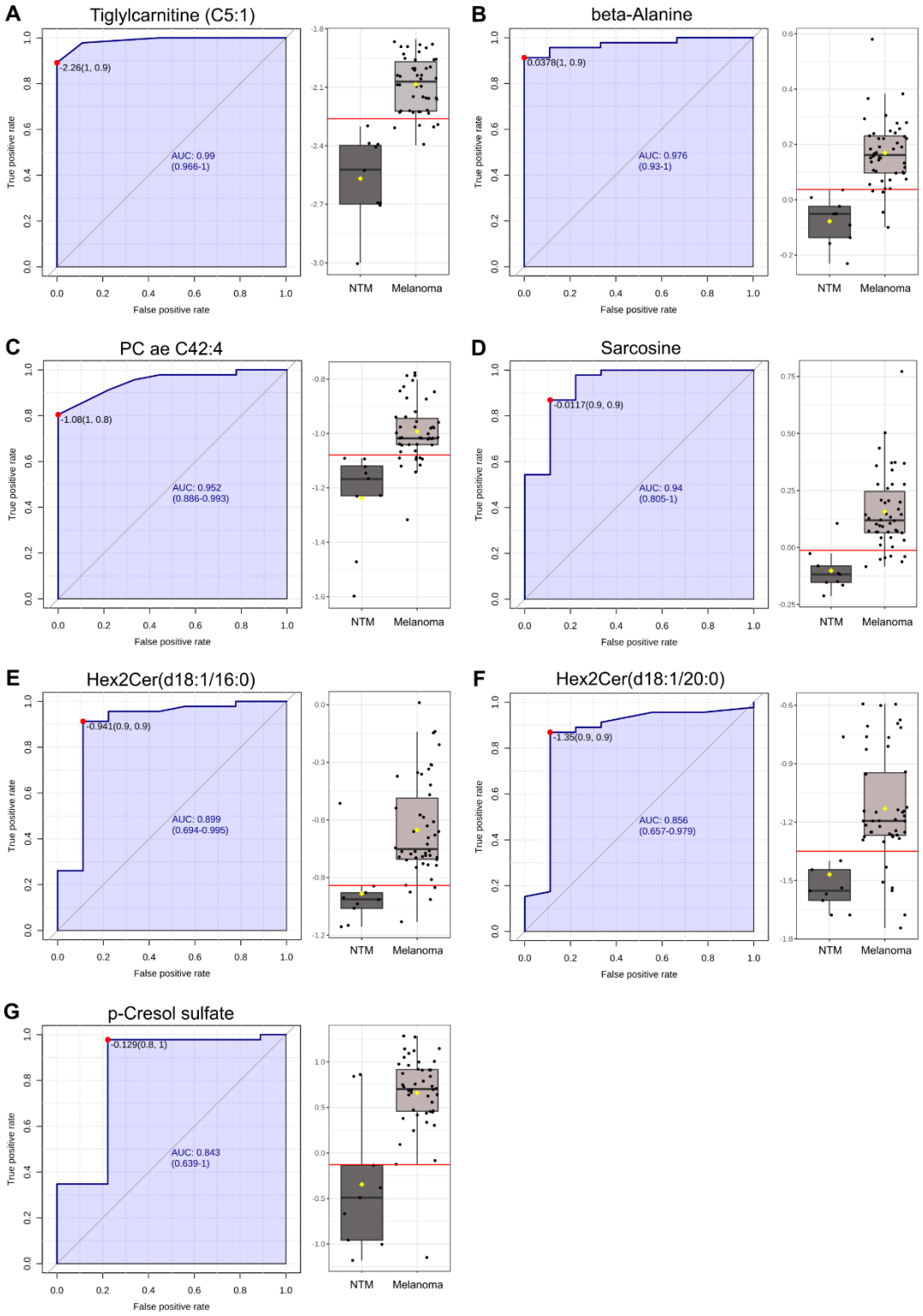

Figure S15. Predictive performance of potential melanoma biomarker candidates. Individual ROC curve analysis of (**A**) tiglylcarnitine, (**B**) beta-alanine, (**C**) and PC ae C42:4, (**D**) sarcosine, (**E**) Hex2Cer(d18:1/16:0), (**F**) Hex2Cer(d18:1/20:0), and (**G**) p-cresol sulfate. Evaluation is based on the comparison of metabolite concentrations in plasma samples obtained from non-tumor mice (n = 9) versus melanoma-bearing mice (n = 46).

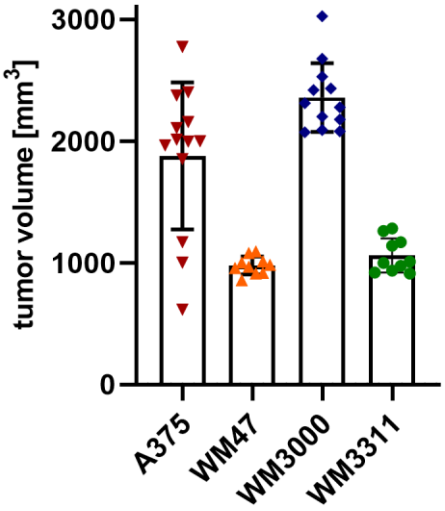

Figure S16. Tumor size of melanoma xenografts. Data represents the tumor volume of A375-, WM47-, WM3000-, and WM3311 melanoma xenografts at the day of collection (n = 10–13).

Table S1. Textual summary of the Venn diagram analysis. The table lists all metabolites which were up- or downregulated in plasma of melanoma vs. non-tumor mice (NTM) in each intersection or were unique to a certain melanoma subtype. Plasma metabolites with an FDR-corrected *p*-value < 0.05 and a fold change >1.5 were included in the analysis performed using the website: http://bioinformatics.psb.ugent.be/webtools/Venn/.

Intersection	**Upregulated Metabolites**		**Downregulated Metabolites**	
	#	Compound	#	Compound
A375 vs. NTM WM3000 vs. NTM WM3311 vs. NTM WM47 vs. NTM	7	beta-Alanine, C5:1, Hex2Cer(d18:1/16:0), Hex2Cer(d18:1/20:0), PC ae C42:4, p-Cresol sulfate, Sarcosine	0	
A375 vs. NTM WM3000 vs. NTM WM47 vs. NTM	2	PC aa C38:6, Trigonelline	1	FA(20:3)
A375 vs. NTM WM3311 vs. NTM WM47 vs. NTM	10	beta-Aminobutyric acid, C16:1-OH, C5-DC, CE(20:5), Choline, EPA, Kynurenine, Taurocholic acid, TG(20:5/34:1), TG(20:5/36:2)	1	Homoarginine
A375 vs. NTM WM3000 vs. NTM WM3311 vs. NTM	2	lysoPC a C26:0, PC aa C24:0	0	
WM3000 vs. NTM WM3311 vs. NTM WM47 vs. NTM	3	Cholic acid, Deoxycholic acid, Taurodeoxycholic acid	0	
A375 vs. NTM WM47 vs. NTM	17	5-Aminovaleric acid, CE(22:6), PC aa C36:5, Symmetric dimethylarginine, TG(16:0/38:6), TG(16:0/40:7), TG(18:1/36:5), TG(18:2/38:5), TG(18:2/38:6), TG(20:3/36:5), TG(20:4/34:2), TG(20:4/36:2), TG(20:4/36:3), TG(20:4/36:4), TG(20:5/36:3), TG(22:6/34:1), TG(22:6/34:2)	2	TG(17:1/32:1), TG(18:1/36:1)
A375 vs. NTM WM3000 vs. NTM	10	Cer(d18:1/16:0), Cer(d18:1/24:1), Cer(d18:2/24:1), Hex3Cer(d18:1/16:0), HexCer(d18:1/16:0), Hippuric acid, PC aa C34:1, PC aa C40:4, PC aa C40:6, PC aa C42:6	11	C3-DC, TG(14:0/36:1), TG(17:0/32:1), TG(18:0/30:1), TG(18:0/32:1), TG(18:0/36:3) TG(18:1/30:0), TG(18:1/31:0), TG(18:1/33:0), TG(18:2/36:0), TG(20:1/32:0)
A375 vs. NTM WM3311 vs. NTM	12	Cer(d18:2/24:0), Glutamate, Hex3Cer(d18:1/18:0), Hex3Cer(d18:1/22:0), HexCer(d18:1/18:1), Lactate, PC ae C40:2, Taurine, TG(20:4/32:1), TG(20:5/34:2), TG(22:5/32:1), TG(22:6/32:1)	0	
WM3000 vs. NTM WM47 vs. NTM	1	C10	1	Carnosine
WM3311 vs. NTM WM47 vs. NTM	9	C4-OH, C5, C6-OH, C8-DC, FA(20:1), Indoxyl sulfate, Proline Betaine, Succinate, TG(16:0/40:8)	2	HexCer(d18:1/18:0), lysoPC a C20:3
WM3000 vs. NTM WM3311 vs. NTM	1	Spermidine	0	

A375 vs. NTM	68	3-Indolepropionic acid, CE(16:0), CE(16:1), CE(18:1), CE(18:2), CE(18:3), Cer(d18:1/22:0), Cer(d18:1/23:0), Cer(d18:1/24:0), Cer(d18:1/25:0), Cer(d18:2/22:0), Cer(d18:2/23:0), DHA, Hex3Cer(d18:1/24:1), HexCer(d18:1/22:0), HexCer(d18:1/23:0), HexCer(d18:1/24:0), HexCer(d18:1/24:1), PC aa C30:0, PC aa C32:0, PC aa C32:1, PC aa C32:2, PC aa C34:2, PC aa C34:3, PC aa C36:2, PC aa C36:6, PC aa C38:0, PC aa C40:2, PC aa C42:0, PC aa C42:1, PC aa C42:4, PC aa C42:5, PC ae C32:1, PC ae C34:2, PC ae C36:4, PC ae C38:0, PC ae C38:1, PC ae C38:2, PC ae C38:6, PC ae C40:6, PC ae C42:0, SM C16:0, SM C24:1, TG(16:0/38:5), TG(16:0/40:6), TG(16:1/36:5), TG(16:1/38:4), TG(16:1/38:5), TG(18:1/38:5), TG(18:1/38:6), TG(18:2/38:4), TG(18:3/38:5), TG(18:3/38:6), TG(20:2/32:1), TG(20:2/34:1), TG(20:2/34:2), TG(20:2/34:3), TG(20:3/34:2), TG(20:3/34:3), TG(20:3/36:3), TG(20:3/36:4), TG(20:4/32:2), TG(20:4/34:1), TG(20:4/34:3), TG(22:4/34:2), TG(22:5/34:2), TG(22:5/34:3), TG(22:6/34:3)	4	TG(16:0/33:1), TG(16:0/35:1), TG(18:0/36:2), TG(20:1/34:0)
WM47 vs. NTM	7	3-Methylhistidine, C3, C4-2M, Iso-C5, Taurochenodeoxycholic acid, Tauromuricholic acid, TG(18:0/36:5)	22	Anserine, Aspartate, DG(18:1/18:1), FA(20:2), lysoPC a C20:4, TG(16:0/35:2), TG(16:0/36:2), TG(16:1/32:1), TG(16:1/34:1), TG(16:1/34:2), TG(16:1/36:1), TG(16:1/36:2), TG(17:1/34:1), TG(17:1/34:2), TG(17:1/34:3), TG(17:2/36:4), TG(17:2/38:5), TG(18:1/32:1), TG(18:1/33:1), TG(18:1/34:1), TG(18:1/35:2), TG(18:1/36:2)
WM3000 vs. NTM	7	CE(22:5), Cer(d18:1/18:0), PC aa C36:4, PC aa C38:5, PC aa C40:5, PC ae C42:2, TG(18:0/38:7)	31	5-Aminovaleric acid, TG(14:0/34:2), TG(14:0/36:3), TG(14:0/36:4), TG(16:0/30:2), TG(16:0/33:2), TG(18:0/30:0), TG(18:0/32:0), TG(18:0/32:2), TG(18:0/34:2), TG(18:1/28:1), TG(18:1/30:1), TG(18:1/30:2), TG(18:1/32:3), TG(18:1/36:6), TG(18:2/28:0), TG(18:2/30:0), TG(18:2/30:1), TG(18:2/32:2), TG(18:2/33:0), TG(18:2/33:1), TG(18:2/33:2), TG(18:2/34:3), TG(18:2/35:1), TG(18:2/35:2), TG(18:2/35:3), TG(18:2/36:1), TG(18:2/36:3), TG(18:3/34:0), TG(18:3/36:1), TG(18:3/36:3)
WM3311 vs. NTM	23	3-Indoleacetic acid, alpha-Aminoadipic acid, Aspartate, beta-Hydroxybutyrate, C3-DC, C4-DC, gamma-Aminobutyric acid, lysoPC a C26:1, TG(16:0/32:1), TG(16:0/33:1), TG(16:0/35:1), TG(16:0/38:1), TG(16:0/38:7), TG(16:1/32:0), TG(17:0/34:1), TG(18:1/28:1), TG(18:1/30:2), TG(18:1/31:0), TG(18:1/32:3), TG(18:1/33:0), TG(18:3/32:0), TG(18:3/32:1), TG(20:1/30:1)	0	

aa: acyl-acyl, ae: acyl-alkyl, Cx:y: x = number of carbons in the fatty acid side chain and y = number of double bonds in the fatty acid side chain, C3: propionylcarnitine, C3-DC: malonylcarnitine, C4-2M: 2-methylbutyrylcarnitine, C4-DC: succinylcarnitine, C4-OH: hydroxybutyrylcarnitine, C5: valerylcarnitine, C5-DC: glutarylcarnitine, C5:1: tiglylcarnitine, C6-OH: hydroxyhexanoylcarnitine, C8-DC: suberyl-carnitine, C10: decanoylcarnitine, C16:1-OH: hydroxyhexadecenoylcarnitine, Cer: ceramide, CE: cholesteryl ester, DG: diglyceride, HexCer: hexosylceramide, Hex2Cer: dihexosyl-ceramide, Hex3Cer: trihexosylceramide, Iso-C5: iso-valerylcarnitine, lysoPC: lyso-phosphatidylcholine, PC: phosphatidylcholine, SM: sphingomyelin, TG: triglyceride, #: indicates the number of up- or downregulated metabolites per intersection.

Supplementary Files 1–4. are provided separately, attached as excel files.



Copyright: © 2021 by the authors. Licensee MDPI, Basel, Switzerland. This article is an open access article distributed under the terms and conditions of the Creative Commons Attribution (CC BY) license (http://creativecommons.org/licenses/by/4.0/).